Inorganic Chemistry
Article

Inorg. Chem. **2009**, *48*, 9085–9091 **9085**
DOI: 10.1021/ic900482v

Synthesis Temperature Effect on the Structural Features and Optical Absorption of $Zn_{1-x}Co_xAl_2O_4$ Oxides

M. Gaudon,* A. Apheceixborde, M. Ménétrier, A. Le Nestour, and A. Demourgues

Institut de Chimie de la Matière Condensée de Bordeaux, UPR 9048 CNRS, 87 Avenue du Dr. Schweitzer, 33608 Pessac Cedex, France

Received March 11, 2009

Zinc/cobalt aluminates with spinel-type structure were prepared by a polymeric route, leading to a pure phase with controlled grain size. The prepared pigments were characterized by powder X-ray diffraction Rietveld analyses in order to determine structural features, scanning electron microscopy for morphological investigation, helium pycnometry and ^{27}Al MAS NMR in order to highlight the occurrence of defects inside the structure, and UV−visible−near-IR spectroscopy to identify electronic transitions responsible for the compounds' color. The green-blue coloration of these pigments is known to be dependent on the sample thermal history. Here, for the first time, the $Zn_{1-x}Co_xAl_2O_4$ color is newly interpreted. The pigment is green once synthesized at low temperature (i.e., with diminution of the pigment grain size); this variation was attributed to the appearance of a new absorption band located at about 500 nm, linked to a complex network feature involving Co ions in octahedral sites as well as oxygen and cationic vacancies. Hence, this work shows the possibility of easily getting a nonstoichiometric network with an abnormal cationic distribution from "chimie douce" processes with moderate synthesis temperature, and so various colorations for the same composition.

1. Introduction

Synthetic blue pigments are widely used in the ceramic industry as coloring agents in glazes or porcelain stoneware.[1,2] The traditional source of blue color in a ceramic pigment remains the cobalt ion (Co^{2+}),[3] and it is more particularly incorporated in a spinel network derived from a rock salt structure exhibiting both octahedral and tetrahedral cationic sites. Hereafter, the study deals with a series of $Zn_{1-x}Co_xAl_2O_4$ compositions extensively used as pigments, and this is particularly true for the $CoAl_2O_4$ head composition;[1−15] moreover, $CoAl_2O_4$ is also studied because of its magnetic[4,5] or catalytic properties.[6] The $CoAl_2O_4$ blue pigment exhibits a large range of colorimetric parameters depending on the thermal history of the material.[6−12] Indeed, the $CoAl_2O_4$ composition (known as Thenard's blue) exhibits a sky-blue hue that was more intense after high-temperature treatment[6−13] than after moderate annealing. In five reference reports,[6−10] the authors have all varied the pigment thermal history and have all observed this phenomenon, where the sample is green when low synthesis temperature is applied. Nevertheless, these effects can be explained by considering various and diverging hypotheses: (i) the occurrence of amorphous carbon, (ii) the presence of a CoO/Co_3O_4 impurity phase,[7,11] (iii) a grain-shape influence (taking into account diffusion phenomena),[12,13] or (iv) the cobalt distribution in the network between octahedral and tetrahedral sites.[16,17]

In this study, $Zn_{1-x}Co_xAl_2O_4$ powders, with x ranging from 0 up to 1 (the total solid solution), were elaborated by a Pechini route and then annealed at various temperatures between 800 and 1100 °C. The diffuse-reflectance spectra were recorded for all samples/all annealing temperatures and

*To whom correspondence should be addressed. E-mail: gaudon@icmcb-bordeaux.cnrs.fr.

(1) Dondi, M.; Matteucci, F.; Baldi, G.; Barzanti, A.; Cruciani, G.; Zama, I.; Bianchi, C. L. *Dyes Pigm.* **2008**, *76*(1), 179.
(2) Hudson Winbow, K. H.; Cowley, J. T. *Ceram. Eng. Sci. Proc.* **1996**, *17*(1), 167–172.
(3) Mason, R. K. *Am. Ceram. Soc. Bull.* **1961**, *40*(1), 5–6.
(4) Suzuki, T.; Nagai, H.; Nohara, M.; Takagi, H. *J. Phys.: Condens. Matter* **2007**, *19*(14), 14265.
(5) Tielens, F.; Calatayud, M.; Franco, R.; Recio, J. M.; Pérez-Ramírez, M.; Minot, C. *J. Phys. Chem. B* **2006**, *110*(2), 988–995.
(6) Angeletti, C.; Pepe, F.; Porta, P. *J. Chem. Soc.* **1977**, *73*, 1972.
(7) Zayat, M.; Levy, D. *Chem. Mater.* **2000**, *12*, 2763–2769.
(8) Garcia Casado, P.; Rasines, I. *J. Solid State Chem.* **1984**, *52*, 187.
(9) Monari, G.; Mandefrini, T. *Ceram. Eng. Sci. Proc.* **1996**, *17*(1), 102–110.
(10) Llusar, M.; Forès, A.; Badenes, J. A.; Calbo, J.; Tna, M. A.; Monros, G. *J. Eur. Ceram. Soc.* **2001**, *21*, 1121–1130.
(11) Pozas, R.; Orera, V. M.; Ocana, M. *J. Eur. Ceram. Soc.*, **2004**, submitted for publication.
(12) Li, W.; Li, J.; Guo, J. *J. Eur. Ceram. Soc.* **2003**, *23*, 2289–2295.
(13) Melo, D. M. A.; Cunha, J. D.; Fernandes, J. D. G.; Bernardi, M. I.; Melo, M. A. F.; Martinelli, A. E. *Mater. Res. Bull.* **2003**, *38*, 1559–1564.
(14) Duan, X.; Yuan, D.; Sun, Z.; Luan, C.; Pan, D.; Xu, D.; Lu, M. *J. Alloys Compd.* **2005**, *386*, 311–314.
(15) Cho, W.-S.; Kakihana, M. *J. Alloys Compd.* **1999**, *287*, 87–90.
(16) O'Neill, H. S. C. *Eur. J. Mineralogy* **1994**, *6*, 603–609.
(17) Natasuka, A.; Ikda, Y.; Yamasaki, Y.; Nakayama, N.; Mizota, T. *Solid State Commun.* **2003**, *128*, 85−90.

Published on Web 08/27/2009

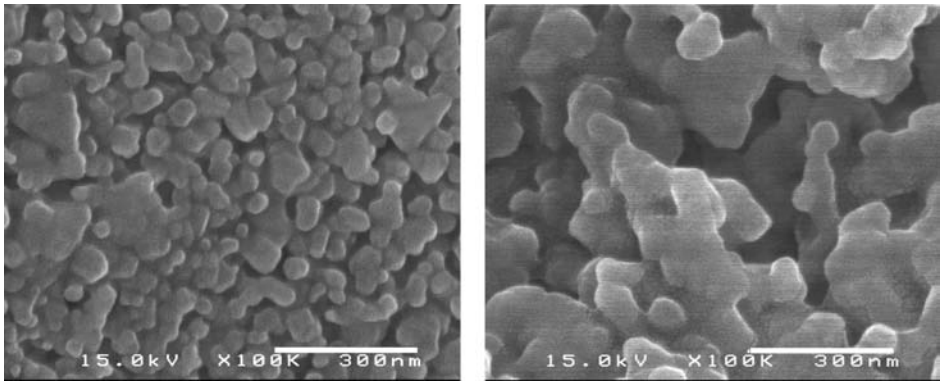

Figure 1. SEM pictures of the $Zn_{0.5}Co_{0.5}Al_2O_4$ composition after annealing at 800 (left) and 1100 °C (right).

interpreted with regard to X-ray diffraction (XRD), pycnometry, and ^{27}Al magic-angle-spinning (MAS) NMR analyses. All synthesized compounds exhibit a spinel type single phase, and hereafter, the results obtained only on several compositions and for two extreme synthesis temperatures: 800 and 1100 °C are discussed. A new interpretation of the color variation of these pigments versus the annealing temperature decrease is thus proposed.

2. Experimental Section

$Zn_{1-x}Co_xAl_2O_4$ pigments were synthesized by the Pechini route.[18] This chemical process is based on cation chelation by citric acid (CA) and on polyesterification between CA and ethylene glycol (EG), which leads to the formation of a polycationic resin. Aqueous solutions of citrate were prepared by dissolving CA in a minimal volume of water. Then, cationic salts $ZnCl_2$ (Aldrich, purity 99.8%), $Co(NO_3)_2 \cdot 6H_2O$ (Aldrich, purity over 99.9%), and $Al(NO_3)_3 \cdot 6H_2O$ (Aldrich, purity 99.9%) were added in stoichiometric proportion to the acid solution. A CA/cations molar ratio equal to 3:1 was used. After complete dissolution of the metallic salts, EG was added with a 4:1 EG/CA molar ratio. EG/CA polymerization was promoted by the removal of water with continuous heating on a hot plate. Then, the highly viscous mixtures were thermally treated in two steps: a first calcination step at 300 °C for 10 h and then an annealing step for 20 h between 800 and 1200 °C.[19]

XRD measurements were carried out on a PANalytical X'PERT PRO diffractometer equipped with an X-celerator detector, using Co $K\alpha_1/K\alpha_2$ radiation ($\lambda_{average} = 1.7909$ Å) to avoid the fluorescence of Co ions/atoms when a copper source is used. The spectra were recorded in the 5−120° 2θ range with a time per step chosen in order to get 10 000 cps in intensity for the main diffractogram peak. Diffractograms were refined with the Rietveld refinement method using the *FULLPROF* program package.[17] The unit cell parameters, atomic positions, cationic distribution (cation inversion parameter), and Debye−Waller factors (isotropic displacements factors) were then refined on the basis of the $Fd\bar{3}m$ space group corresponding to the spinel structure. The peak profiles are fitted with the Caglioti function, i.e., considering isotropic crystallites. Uncertainties can be calculated from the standard deviation proposed by the software; with these uncertainties being approximated in all cases to the decade higher, all reported results are limited to their last significant digit. Hence, the standard deviation is absent of the relevant tables.

(18) Pechini, N. U.S. Patent 3,330,697, **1967**.
(19) Rodriguez-Carvajal, J. *Abstracts of the Satellite Meeting on Powder Diffraction of the XV Congress of the IUCr*, Toulouse, France, **1990**, p 127.

The morphology of the $Zn_{1-x}Co_xAl_2O_4$ nanoparticles was roughly evaluated by scanning electron microscopy (SEM). For the sample preparation, the powder was ultrasonicated in ethanol and then a droplet of the suspension was deposited and dried on the sample support. SEM micrographs were recorded with a Hitachi 4500-I apparatus fit out with a field-emission gun working at 3.0 kV. Such equipment allows a high spatial resolution (roughly equal to 5 nm).

Density measurements on powdered samples (with the oxide crystallite density being considered as the experimental to theoretical crystallite specific weight) were performed with a micromeritics helium pycnometer (Accupyc II 1340 model series) with at least 500 mg of powder inside cells of 1 cm^{-3} volume. The standard deviation was directly calculated from the 10 measurements performed and proposed by the software of the apparatus; thus, it allowed determination of the error bars on reported values: 0.005 $g \cdot cm^{-3}$ was estimated here as the error bar (i.e., about 1% relative error).

^{27}Al MAS NMR spectra were recorded using a Bruker Avance 500 solid-state spectrometer at 130.3 MHz. The spinning speed was 30 kHz using 2.5 mm zirconia rotors. A single pulse sequence was utilized with a 1 μs pulse duration corresponding a $\pi/12$ flip angle for a liquid sample. The spectral width was 1 MHz, and the recycle time was 30 s. The 0 ppm reference was set to a 1 M aluminum nitrate solution using a secondary solid-state reference of $Al(PO_3)_3$ (−21.4 ppm).

Diffuse absorbance spectra, presented here after Kubelka−Munk transformation, were recorded at room temperature from 200 to 800 nm with a step of 1 nm and a band length of 2 nm on a Cary 17 spectrophotometer using an integration sphere. Halon was used as a white reference for the blank. A mathematical treatment of the obtained spectra allowed determination of the L*a*b* space colorimetric parameters. The first step of the treatment consisted of obtaining the *XYZ* tristimulus values (defined by the CIE, 1964) from the integration (on the visible range, i.e., from $\lambda = 380$ up to 780 nm) of the product of $x(\lambda)$, $y(\lambda)$, or $z(\lambda)$ functions (CIE, 1964) with the diffuse-reflectance spectra function $X = \int x(\lambda)\, R(\lambda)\, d\lambda$. Then, the transfer equations defined by the CIE, 1976, from the *XYZ* space to the L*a*b* space, were used in order to obtain the L*a*b* chromatic parameters.

3. Results and Discussion

3.1. Structural Investigations. Annealing causes a particle growth that is easy to diagnose from SEM analyses. In Figure 1, it is clearly shown that the particles are more individualized after annealing at 800 °C than after that at 1100 °C, with sintering necks being more developed after the highest temperature treatment. The "individual" particles seem to correspond to single crystalline grains, with

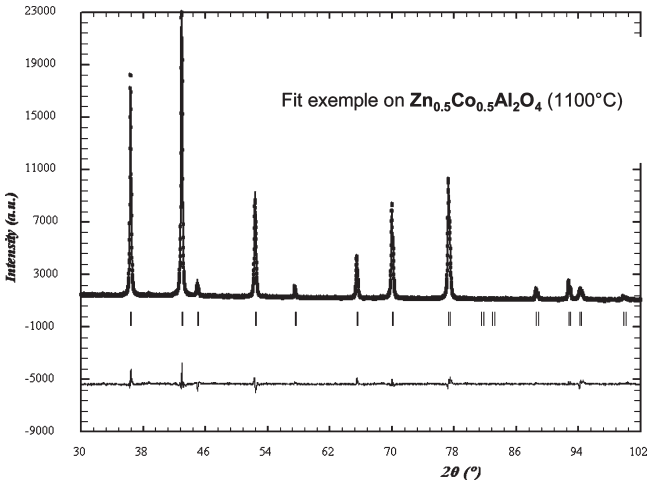

Figure 2. Rietveld refinements of the $Zn_{0.5}Co_{0.5}Al_2O_4$ composition annealed at 1100 °C.

characteristic sintering necks being formed between the particles. Their sizes were evaluated as about 40 and 150 nm for 800 and 1100 °C annealing treatments, respectively.

XRD investigations were performed on the three compositions $ZnAl_2O_4$, $Zn_{0.5}Co_{0.5}Al_2O_4$, and $CoAl_2O_4$ obtained after annealing at 800 and 1100 °C. A graphical illustration of the experimental, calculated, and difference signals issued from a Rietveld fit is reported in Figure 2 for the intermediate composition. The spinel-type structure adopts the $Fd\bar{3}m$ space group with $A^{2+}{}_{1-\gamma}B^{3+}{}_{\gamma}[A^{2+}{}_{\gamma}B^{3+}{}_{2-\gamma}]O_4$ composition, with γ representing the inversion parameter (the cation interbrackets correspond to the octahedral sites). The results obtained for the three compositions (*a* cell parameters, *x*,*x*,*x* oxygen atomic position, isotropic displacement factors, inversion parameter, and reliability factors) are all reported in Table 1. The refinement was performed by considering no atomic vacancy. Furthermore, for the intermediate composition $Zn_{0.5}Co_{0.5}Al_2O_4$ and from the difficulty in distinguishing Zn^{2+} and Co^{2+} ions because of their electronic configuration proximity, the inversion parameter was applied only on the Co^{2+} ions; indeed, the extreme $CoAl_2O_4$ and $ZnAl_2O_4$ compositions show that the Co ions have an inversion parameter largely superior to the Zn ones. Moreover, from the Debye−Scherer equation, the particles size can be approximated from the full width at half-maximum of the diffraction peaks (knowing the instrumental broadening) to about 30 nm for the 800 °C treated powder and over 100 nm for the 1100 °C treated sample for each composition. These results confirm the previous observation made with the SEM analyses. From a structural point of view, several observations can be made. (i) Here, the soft chemistry route followed by a low annealing temperature leads to compounds exhibiting peculiar cell parameters. Indeed, for all three compositions studied, the cell parameters of the compounds obtained at low temperature are abnormally smaller than those of compounds obtained at $T = 1100$ °C. Only one explanation can be proposed considering the following arguments: these compounds exhibit vacancies. From a thermodynamic point of view, the increase of the preparation temperature can only lead to an increase of the compound stability, i.e., to a crystal energy decrease. Moreover, for a determined composition, the denser the structural network, the more stable it is. In our case, the densities of the samples annealed at high temperatures are therefore higher (or equal) than the low-temperature ones. Then, while the annealing temperature increases, the simultaneous increase of the density and cell volume shows that vacancies are present in low-thermal-treatment oxides. It seems that the compound *reduces its atomic vacancies* only at very high temperatures. Hence, spinel compounds obtained for low-temperature syntheses (just after its crystallization) exhibit a lacunar structural framework. Furthermore, as the cobalt content increases, the inversion parameter increases too. This result was readily accessible compared to the structural data of the literature on $CoAl_2O_4$ or $ZnAl_2O_4$.[20,21] Moreover, as the cobalt fraction increases, the cell parameter increases, which is consistent with the literature data.[20,21] Indeed, the 1100 °C treated samples have structural parameters roughly corresponding to those already reported for the same composition, with the "abnormal" set of parameters corresponding to the 800 °C treated compounds. Nevertheless, it is still surprising that the cell parameter increases with the cobalt fraction because Co^{2+} ions are slightly smaller than Zn^{2+} ions: cation−oxygen distances in tetrahedral environments issued from the Brown and Altermatt model[22] are respectively 1.95 and 1.96 Å. Ideal direct spinels, i.e., exactly satisfying the various ionic sizes of the cations involved, would exhibit a cell parameter of 8.084 Å for the $ZnAl_2O_4$ composition and 8.060 Å for the $CoAl_2O_4$ one. The cell parameter and γ inversion parameter variation with the cobalt content as well as the network densification versus preparation temperature lead us to estimate that, upon cobalt substitution for zinc, the increase of the cell parameters is due to an increasing amount of cationic vacancies from the pure cobalt spinel to the pure zinc one. Finally, the isotropic displacement factors tend to decrease in a reproducible way versus the synthesis temperature. However, they are independent of the spinel composition. The higher Debye−Waller factors found for the 800 °C treated compounds can be a consequence of the occurrence of a higher inversion parameter as well as numerous vacancies inducing a significant local disorder on each position.

3.2. Helium Pycnometry. Helium pycnometry giving direct access to density was performed in order to confirm the presence of numerous atomic vacancies in the spinel network elaborated via moderate temperature. Analyses have confirmed that a lower synthesis temperature for the various compositions leads to significantly smaller specific weights than the theoretical ones. Indeed, on the basis of the results reported in Figure 3, it can be observed that, for each analyzed composition (here for $x = 0$, 0.2, 0.5, and 1), the oxide densities after the 1100 °C heat treatment (ranging between 97 and 100%) are higher than those observed after the 800 °C heat treatment (between 93 and 97%). The second observation is that, for the same

(20) Christensen, A. N.; Norby, P.; Hanson, J. C. *Powder Diff.* **1995**, *10*, 185–188.
(21) Garcia Casado, P.; Rasines, I. *J. Solid State Chem.* **1984**, *52*, 187–193.
(22) Brown, I. D.; Altermatt, D. *Acta Crystallogr.* **1985**, *B41*, 244–247.

Table 1. Cell Parameters, Atomic Positions, Displacements, Cation Inversion Parameters, and Reliability Factors of the Various Compositions Synthesized

composition	annealing T, °C	a (Å)	32e position	B_{iso} (per site) (Å^2)	γate	reliabilty factors
$ZnAl_2O_4$	800	8.0808	0.264	0.8 (8a), 0.8 (16d), 0.7 (32e)	4%	C_{Rp} = 11%, C_{Rwp} = 14%, R_{Bragg} = 4.5
	1100	8.0846	0.264	0.6 (8a), 0.6 (16d), 0.5 (32e)	4%	C_{Rp} = 10%, C_{Rwp} = 11%, R_{Bragg} = 2.6
$Zn_{0.5}Co_{0.5}Al_2O_4$	800	8.0906	0.267	1.0 (8a), 1.0 (16d), 0.8 (32e)	11%	C_{Rp} = 13% C_{Rwp} = 15%, R_{Bragg} = 5.5
	1100	8.0952	0.267	0.3 (8a), 0.3 (16d), 0.2 (32e)	10%	C_{Rp} = 10%, C_{Rwp} = 11%, R_{Bragg} = 2.7
$CoAl_2O_4$	800	8.0995	0.265	0.5 (8a), 0.8 (16d), 0.6 (32e)	19%	C_{Rp} = 12%, C_{Rwp} = 11%, R_{bragg} = 2.9
	1100	8.1051	0.264	0.3 (8a), 0.6 (16d), 0.3 (32e)	12%	C_{Rp} = 12%, C_{Rwp} = 12%, R_{bragg} = 2.8

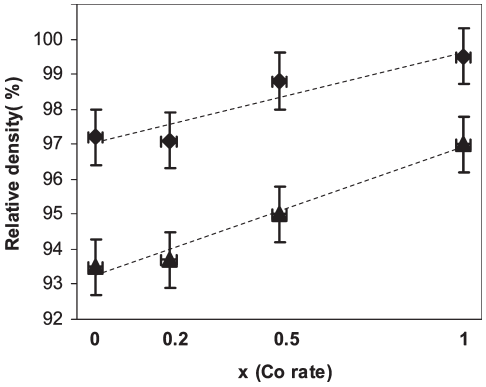

Figure 3. Density measured by helium pycnometry measurements for two sets of compounds (▲, 800 °C treated compounds; ◆, 1100 °C treated compounds).

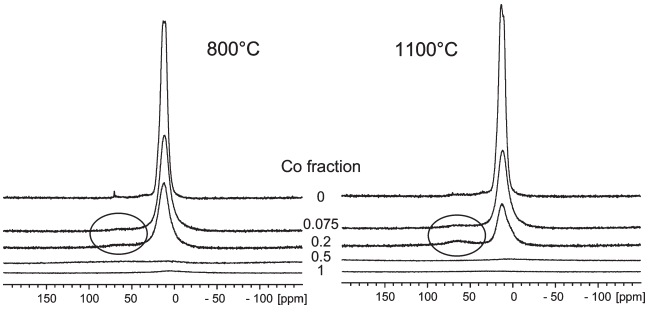

Figure 4. ^{27}Al MAS NMR spectra for the two series of $Zn_{1-x}Co_xAl_2O_4$ compounds prepared at 800 °C (left) and 1100 °C (right). All of the spectra are plotted on a common intensity scale normalized to the mass of the NMR samples. Only the central isotropic peaks are shown; the signals for tetrahedral Al coordination are circled.

thermal treatment, the oxide density slightly increases versus the cobalt rate ($\Delta\rho/\rho \approx 4\%$ from $ZnAl_2O_4$ to $CoAl_2O_4$ for an annealing temperature equal to 800 °C). A dense framework seems thus more difficult to reach with Zn and Al atoms than with Co and Al ones. The density evolution can be correlated to the cell parameter evolution. When the compound contains cationic vacancies, the spinel cell volume appears to be lower compared to a globally similar composition with denser network packing.

3.2. Al NMR Studies. ^{27}Al MAS NMR spectroscopy gives supporting information on the various Al local environments/coordination. Signals for the compositions $x = 0$, 0.125, 0.2, and 0.5 and for samples synthesized at 800 and 1100 °C are reported in Figure 4. The ^{27}Al MAS NMR signals are mainly constituted of an intense peak characteristic of a 6-coordinated site. When the cobalt content increases, the signal intensity drastically decreases until nearly a complete disappearance for $x =$ 0.5. For some of the samples, a slight inversion depicted by the presence, at 70 ppm, of a small peak corresponding to 4-coordinated Al can be clearly seen. These 4-coordinated Al characteristic peaks are most visible after 1100 °C annealing. On the opposite side, the characteristic peak of 6-coordinated Al ions is significantly smaller for the 1100 °C annealed samples than for the 800 °C ones (for any given composition).

The rapid disappearance of the 6-coordinated Al signal must be due to magnetic interactions between the paramagnetic Co^{2+} ions and the Al^{3+} ones. On the basis of the investigation of the mechanisms of such interactions,[23,24] they can a priori occur from octahedral Co^{2+} ions with the high-spin $t_{2g}{}^5e_g{}^2$ electronic configuration because the t_{2g} orbitals containing one paramagnetic spin points directly toward the Al nucleus sitting on the edge-sharing octahedron (direct t_{2g} interactions); the e_g electron spins point to the oxygen and therefore would only interact with corner-sharing octahedra, which are not present in spinel-type form. It can also occur from tetrahedral Co^{2+} with the $e^4t_2{}^3$ configuration, although in such a case, the mechanism for the transfer of the electron spin density is less clear (120° Co−O−Al). In order to know which of these interactions really leads to the extinction of the neighboring octahedral Al NMR signal, the experimental peak area for various cobalt concentrations ($x_{Co} = 0$, 0.075, and 0.2) was measured after annealing at 800 and 1100 °C. These areas are expressed in percentage considering 100% as the area of the $x = 0$ signal, which is similar for both annealing temperatures. Then, we calculated the theoretical areas from binomial law considering that either the octahedral Co or the tetrahedral Co, or both, leads to extinction of the signal of the neighboring Al octahedral sites for various cobalt contents (x_{Co}) and various cobalt inversion parameters (γ_{Co}). The calculated areas can be easily expressed as a percentage of the $x = 0$ signal and so can be directly compared to the previous ones. For instance, the area (%) of the 6-coordinated Al^{3+} signal in case i, for which only the direct t_{2g} "octa−octa" interactions are active, is A_{O-O} % = $100(1 - x_{Co}\gamma_{Co}/2)^6(1 - x_{Co}\gamma_{Co}/2)$, where $x_{Co}\gamma_{Co}/2$ represents the octahedral site fraction occupied by Co^{2+} ions, $1 - x_{Co}\gamma_{Co}/2$ the octahedral site fraction occupied by Al^{3+} ions, and $(1-x_{Co}\gamma_{Co}/2)^6$ the probability for an octahedral ion to get only Al^{3+} edge-sharing octahedral sites, with an octahedral site getting six first-neighboring octahedral sites. In the same way, in case ii, for which only the 120° "tetra−octa" interactions are active, $A_{O_h-O_h}$ % = $100(1 - x_{Co}[1 - \gamma Co])^6(1 - x_{Co}\gamma_{Co}/2)$, and finally, in case iii, for which both interactions are

(23) Carlier, D.; Menetrier, M.; Grey, C. P.; Delmas, C.; Ceder, G. *Phys. Rev. B* **2003**, *67*(17), 1–14.
(24) Chazel, C.; Ménétrier, M.; Carlier, D.; Croguennec, L.; Delmas, C. *Chem. Mater.* **2007**, *19*(17), 4166–4173.

Table 2. Experimental and Calculated Areas from Binomial Law of the Peak Relative to the 6-Coordinated Aluminium (Error Bars on the Relative Areas Are Estimated To Be about 1%)

	experimental areas (%)					
x_{Co}	T = 800 °C	T = 1100 °C	γ_{Co}	area if "octa−octa" interactions	area if "tetra−octa" interactions	area if "both" interactions
0	100			100	100	100
0.075	79	68	0	100	63	63
			0.2	93	68	65
			0.5	88	78	69
			1	76	96	76
0.2	62	38	0	100	26	26
			0.3	81	39	32
			2/3	62	61	41
			1	48	91	48
0.5	≪5	≪5	0	100	1.5	1.5
			0.5	58	7	4

active, $A_{O_h-O_h+O_h-T_d}$ % $= (1 - x_{Co}\gamma_{Co}/2)^7(1 - x_{Co}[1 - \gamma_{Co}])^6$. These measured and calculated areas are both reported in Table 2. By direct comparison, one can observe the following: (i) The significant collapse of the signal versus cobalt concentration can only be explained by the action of 120° "tetra−octa" interactions. (ii) On the opposite side, the significant evolution of the signal intensity for the same cobalt concentration versus the annealing temperature shows that the 90° "octa−octa" interactions are not efficient; moreover, the signal detected notably after 800 °C annealing is significantly too intense considering that "both" interactions are efficient,. Thus, the fit of the experimental and calculated areas considering binomial law with only 120° "tetra−octa" interactions allows extraction of the cobalt inversion parameter. For instance, this inversion parameter is roughly 0.2 for the $x = 0.075$ composition obtained after annealing at 1100 °C. For a given thermal history, the inversion parameter slightly increases versus the doping concentration, consistent with what was shown by XRD analyses; however, for the same composition, this parameter seems to significantly decrease with the annealing temperature, whereas X-ray analyses had not revealed an annealing temperature influence for the low cobalt content. The difficulty is to differentiate Co^{2+} and Zn^{2+} occupancies in T_d and O_h sites by XRD analyses.

Moreover, it can be seen in Figure 4 that the signals exhibit a second peak, which can be attributed to aluminum in tetrahedral sites from the literature. This peak, whatever the composition, is very weak and difficult to quantify by integration; nevertheless, it is clear that, whatever the composition, its intensity is more significant for the high-temperature annealed samples than for the low-temperature ones. Hence, even if cobalt occupies in larger amount the octahedral site after annealing at 800 °C (the X-ray results on the $CoAl_2O_4$ composition lead clearly to this information), aluminum occupies in larger amount the tetrahedral one at 1100 °C (from NMR analyses, whatever the Zn/Co composition). Actually, zinc is without a doubt the key point for the interpretation of these two observations, being in a first point of view in the orthogonal positions. Indeed, between the samples annealed at 800 and 1100 °C, the zinc fraction in the octahedral sites seems to vary a lot and in an opposite way in comparison with the cobalt one. Such a hypothesis also explains why from XRD the "global" inversion parameter deduced from electronic densities is nearly constant versus the annealing temperature, whereas significant changes are detected by ^{27}Al NMR analyses. Moreover, the zinc atomic distribution, cationic vacancies, here not taken into account, can have a variable site distribution depending on the sample thermal history.

3.3. Colorimetric Investigations. The K/S absorption spectra recorded in the near-UV−visible−near-IR range are reported in Figure 5. The triple d−d band appearing at about 600 nm is relative to the Co^{2+} ion in the tetrahedral site. Indeed, for tetrahedral symmetry, considering the Tanabe−Sugano diagrams established for a $3d^3$ electronic configuration (in 4-fold coordination, the d^{10-n} Tanabe−Sugano diagram has to be considered), this triple band was indexed as a $^4A_2 \rightarrow {}^4T_1$ transition, which decomposes as a triplet due to the L−S Russel−Saunders coupling, for which the maximal absorptions, for instance, in $CoAl_2O_4$, are near 540, 590, and 640 nm.[10] The intensity of this triple band increases, whatever the composition, from 800 to 1100 °C annealing; this traduces the increase of the cobalt fraction in the tetrahedral sites with increasing calcination temperature, as was also shown from NMR experiments, whatever the samples. A gap associated with ligand (oxygen anion)-to-metal (cobalt and/or zinc cations) electronic transfer can be seen near the UV−visible frontier. Furthermore, for the low annealing temperature (800 °C), an additional absorption band whose intensity increases versus the cobalt concentration appears at about 350−400 nm (reported as ◆ in Figure 5). This band is relatively broad. For instance, for $x = 0.5$, i.e., a high cobalt concentration, the spread of this band is prolonged until 750 nm. In all cases, this well-defined new absorption band shows that the pigment coloring variation is not due to a diffusion aspect linked to particle sizes or carbon traces, i.e., explanations already proposed in the literature.[6−10] Without a doubt, this band is linked to the fact that cobalt ions (the unique chromophore ions) either possess a new oxidation degree or are located inside new sites (interstitial and/or octahedral sites). The perfect stability of the color while the compound is annealed under an argon atmosphere (with the experiment being followed by thermogravimetry with no weight loss detected) shows that Co^{3+} ions are not involved. Also, the location of the Co^{2+} cations in

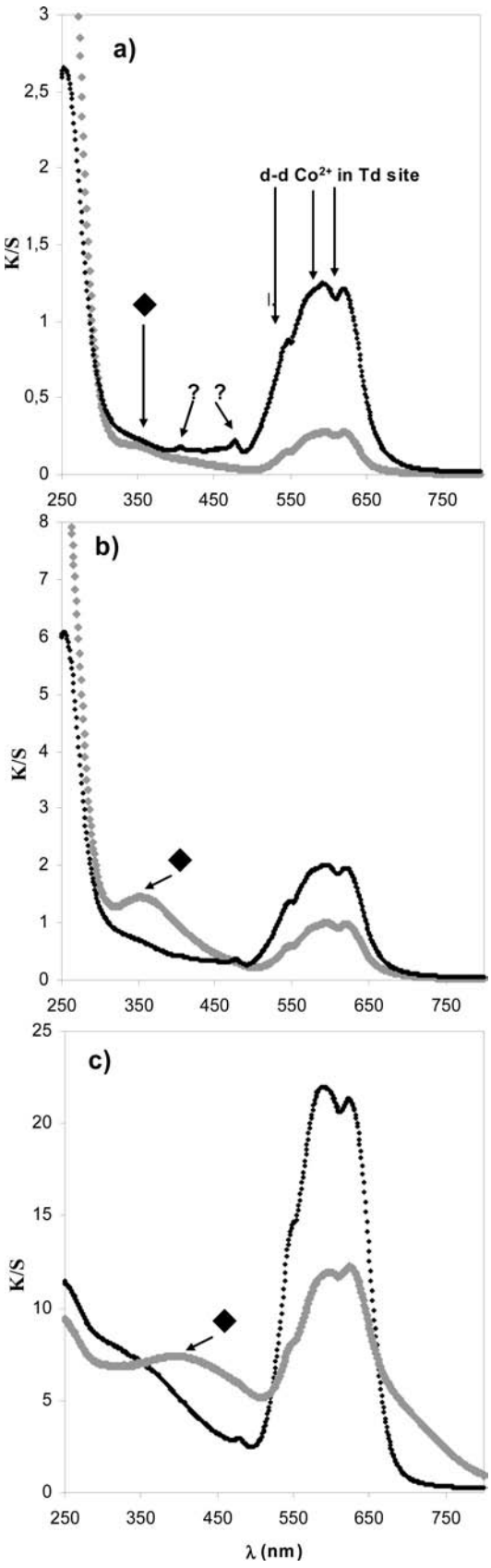

Figure 5. K/S absorption spectra of (a) $Zn_{0.925}Co_{0.075}Al_2O_4$, (b) $Zn_{0.8}Co_{0.2}Al_2O_4$, and (c) $Zn_{0.5}Co_{0.5}Al_2O_4$ compositions annealed at 800 °C (gray curve) or 1100 °C (black curve).

"standard" octahedral sites cannot be responsible for this band apparition because the d−d transitions associated

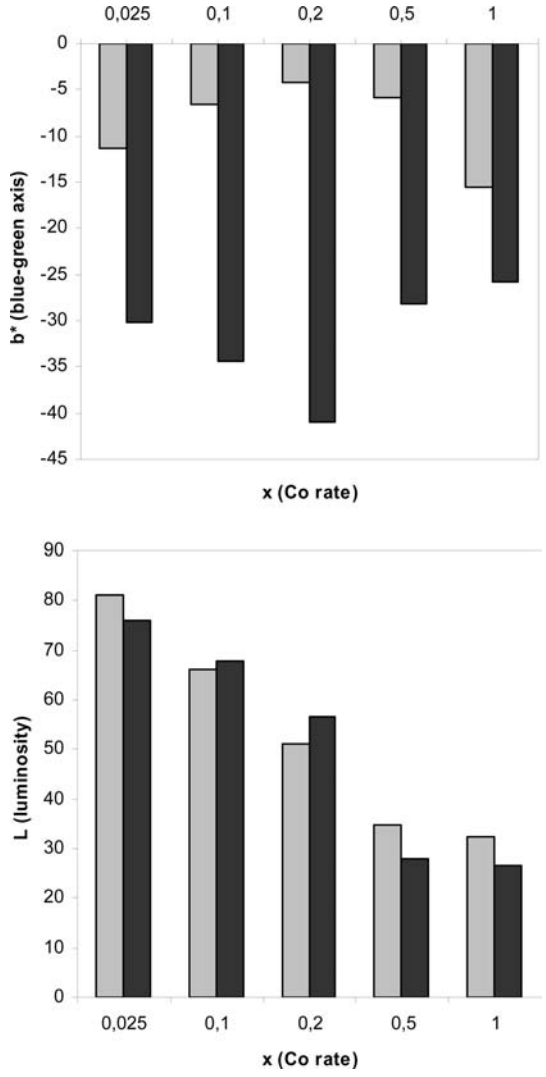

Figure 6. L^* and b^* coloring parameters for various cobalt concentrations and for 800 °C (gray bars) and 1100 °C (black bars).

with this ion in such a configuration are known to be centered at about 1300 nm ($^4F \rightarrow {}^4T_2$), 720 nm ($^4F \rightarrow {}^4A_2$), and 550 nm ($^4F \rightarrow {}^4T_2$, second excited state), leading, hence, to a violet coloration. Thus, with regard to the above discussions and the cationic distribution previously characterized, this new band could be due to the positioning of Co^{2+} ions in the spinel B sites but strongly modified: maybe defective sites with a local 5-coordination. The mechanism intraatomic electron transfer (due to the crystal field around the cobalt) or interatomic electron transfer (charge-transfer band from an oxygen through the cobalt) remains unclear.

From the colorimetric point of view, the variation from green to blue color versus the annealing temperature leads to the b^* parameter evolution: the b^* parameter increases from a very low value (for a greenish hue, the b^* parameter characteristic of the blue-yellow axis is very near 0) to high values (for saturated blue). Figure 6 shows the measured b^* parameter for various $Zn_{1-x}Co_xAl_2O_4$ compositions and for the two annealing temperatures 800 and 1100 °C. The brightness (L^*), which logically decreased with the cobalt concentration (with cobalt being the only absorptive species), and the a^* chromatic parameter also shift versus

the annealing temperatures but in a less significant way. One can distinguish an "optimal" cobalt concentration for which the b^* contrast between the 800 and 1100 °C annealed samples is the highest ($x = 0.2$). This critical concentration should correspond to the largest change of the relative cationic distribution of the cobalt species inside the spinel network between the two annealing temperatures.

4. Conclusion

The Co-based spinels ($Zn_{1-x}Co_xAl_2O_4$) are known to exhibit a green or blue color depending on their synthesis history; in this paper, this phenomenon is newly interpreted and controlled in order to produce various pigment hues. The phenomenon responsible for such a color variation is very complex. First, it was shown that the Co ions, with only a Co^{2+} oxidation state, are located in larger proportions in the octahedral sites for low synthesis temperatures than for high ones (^{27}Al MAS NMR and UV−visible spectroscopy). Second, for a low cobalt concentration, few Al^{3+} ions occupy the tetrahedral sites and the Zn^{2+} ions, which are more difficult to individually characterize, should be located in higher proportions in the tetrahedral sites for low synthesis temperatures and in octahedral ones for high synthesis temperatures, i.e., opposite to that of the cobalt ions (XRD and ^{27}Al MAS NMR). Third, some vacancies are present inside the spinel structure: they have to be both anionic and cationic for charge compensation; the vacancy fraction decreases with the synthesis temperature and also slightly decreases with the cobalt concentration (helium pycnometry and XRD). These vacancies can also have a distribution on the tetrahedral and octahedral sites that varies versus the thermal treatment temperature. One important and interesting consequence of these points is the strong modulation of the color of these compounds with the synthesis temperature. A more detailed investigation by visible spectroscopy revealed that the color is strongly tailored by an absorption band that can only be attributed to Co^{2+} ions inside a strongly modified B site, probably with a local 5-coordination. Moreover, the fundamental interest of this new interpretation is for the desired green coloration of $Zn_{1-x}Co_xAl_2O_4$ oxides for low synthesis temperature; this study opens the way for applications based on the ability of these green-blue cobalt spinels to change in an irreversible way their color during post-thermal treatment. Hence, one can understand that they can be used as "thermal history recorders", for example, in motorization characterization, offset impression, alarm inks on hot systems, etc. In this sense, an optimal composition ($x = 0.2$), exhibiting a larger optical contrast versus treatment temperature, was distinguished here.